Quantification Techniques to Minimize the Effects of Native T_1 Variation and B_1 Inhomogeneity in Dynamic Contrast-Enhanced MRI of the Breast at 3 T

Che A. Azlan,[1,2]* Trevor S. Ahearn,[1] Pierluigi Di Giovanni,[1] Scott I. K. Semple,[3] Fiona J. Gilbert,[1] and Thomas W. Redpath[1]

The variation of the native T_1 (T_{10}) of different tissues and B_1 transmission-field inhomogeneity at 3 T are major contributors of errors in the quantification of breast dynamic contrast-enhanced MRI. To address these issues, we have introduced new enhancement indices derived from saturation-recovery snapshot-FLASH (SRSF) images. The stability of the new indices, i.e., the SRSF enhancement factor (EF_{SRSF}) and its simplified version (EF'_{SRSF}) with respect to differences in T_{10} and B_1 inhomogeneity was compared against a typical index used in breast dynamic contrast-enhanced MRI, i.e., the enhancement ratio (ER), by using computer simulations. Imaging experiments with Gd-DTPA-doped gel phantoms and a female volunteer were also performed. A lower error was observed in the new indices compared to enhancement ratio in the presence of typical T_{10} variation and B_1 inhomogeneity. At changes of relaxation rate (ΔR_1) of 8 s^{-1}, the differences between a T_{10} of 1266 and 566 ms are <1, 12, and 58%, respectively, for EF_{SRSF}, EF'_{SRSF}, and ER, whereas differences of 20, 8, and 51%, respectively, result from a 50% B_1 field reduction at the same ΔR_1. These quantification techniques may be a solution to minimize the effect of T_{10} variation and B_1 inhomogeneity on dynamic contrast-enhanced MRI of the breast at 3 T. Magn Reson Med 67:531–540, 2012. © 2011 Wiley Periodicals, Inc.

Key words: DCE-MRI; high-field MRI; native T_1; B_1 inhomogeneity

Dynamic contrast-enhanced (DCE)-MRI is the most sensitive imaging technique available for the detection and characterization of breast cancers (1–3). By using a T_1-weighted pulse sequence a tumor will show a greater postcontrast signal than normal tissues. The abnormal vasculature of the tumor allows preferential accumulation of contrast agent in the tumor extravascular extracellular space, shortening the longitudinal relaxation time (T_1), and resulting in tumor signal enhancement.

[1]Aberdeen Biomedical Imaging Centre, University of Aberdeen, Aberdeen, Scotland, United Kingdom.

[2]Department of Biomedical Imaging, University of Malaya, Kuala Lumpur, Malaysia.

[3]Clinical Research Imaging Centre, University of Edinburgh, Edinburgh, Scotland, United Kingdom.

*Correspondence to: C. A. Azlan, Ph.D., Aberdeen Biomedical Imaging Centre, University of Aberdeen, Lilian Sutton Building, Foresterhill, Aberdeen AB25 2ZD, Scotland, United Kingdom. E-mail: azlanbme@um.edu.my

Received 19 November 2010; revised 22 April 2011; accepted 4 May 2011.

DOI 10.1002/mrm.23021

Published online 7 June 2011 in Wiley Online Library (wileyonlinelibrary.com).

However, the postcontrast to precontrast signal difference is dependent on imaging factors such as preamplifier gain and voxel size. Hence, to standardize the measurement of signal enhancement, the postcontrast signal is referred to a baseline parameter, which is unaffected by the contrast agent. In practice, usually the signal enhancement is normalized to the precontrast T_1-weighted signal. In this article, we refer to this enhancement index as the enhancement ratio (ER)

$$\mathrm{ER} = \frac{S_{\mathrm{POST}} - S_{\mathrm{PRE}}}{S_{\mathrm{PRE}}}, \qquad [1]$$

where S_{PRE} and S_{POST} are the T_1-weighted signals obtained before and after the contrast agent injection, respectively.

For convenience, the increase in signal intensity is often assumed to be directly (or at least approximately) proportional to the changes in relaxation rate (ΔR_1) of the tissue. Therefore, the signal enhancement is approximately linearly related to the contrast agent uptake of the tissue. To illustrate the problem we wish to address, consider that we have two tissues that take up the contrast agent equally, so that they have identical changes of R_1 and hence identical changes of absolute signal. The tissue with the lower R_1 precontrast value will therefore enhance from a lower precontrast signal level than will the tissue with the higher R_1 precontrast value. Hence, ER will be higher for the tissue with the lower precontrast R_1. More simply, tissues with longer precontrast T_1 relaxation times tend to have larger ER. Therefore, there is a bias in the index which could affect the diagnostic accuracy of DCE-MRI studies. The relationship between T_{10} and ER may contribute to a greater sensitivity of the DCE-MRI examination where T_{10} is longer than normal. However, this may be at the expense of specificity as T_{10} is not necessarily related to contrast agent pharmacokinetics.

Quantitative analysis may be performed using multicompartment pharmacokinetic modeling of the DCE-MRI enhancement. To account for the effects of native T_1 (T_{10}) on enhancement pharmacokinetic modeling, the T_{10} may be measured before the dynamic MRI scanning and incorporated into the pharmacokinetic model (4). However, the disadvantage of performing T_{10} measurements in vivo is that it can be challenging to implement especially in MR centers with little research expertise. Hence, the technique is rarely incorporated into routine clinical breast DCE-MRI. Another drawback of this technique is significant errors can also be introduced into

the parameters calculated through errors in the T_{10} measurement (5,6). As such a method of measuring signal enhancement that is independent of T_{10} would be beneficial.

At 1.5 T and lower fields, DCE-MRI is typically performed by using a FLASH pulse sequence. This technique produces a good tissue contrast and spatial resolution within an acceptable clinical scanning duration. 3-T MRI is becoming more commonly used in clinical MRI. The main advantage of these high-field scanners is the improvement in image signal-to-noise ratio (SNR). However, the drawback of these scanners is that B_1 transmission-field inhomogeneity is increased in the field-of-view (FOV) (7), which causes a significant error in the calculated ER (8) and pharmacokinetic quantifications (9). To minimize the effect of the B_1 inhomogeneity in DCE-MRI, a saturation-recovery snapshot-FLASH (SRSF) pulse sequence is proposed for imaging. Several workers have used SRSF to minimize B_1-field inhomogeneity effects in their research. Hoffmann et al. (10) used this pulse sequence to improve the temporal resolution of breast DCE-MRI. The technique has also been used to measure the T_{10} of breast tissues (11). At 3 T, this approach has been used by Kim et al. (12) in cardiac imaging. It also has been shown that the SRSF pulse sequence is much less sensitive to the B_1 inhomogeneity when calculating ER (13).

The aim of this study was to develop and evaluate enhancement indices that are insensitive both to the variation of tissues' T_{10} and B_1 transmission-field inhomogeneity in DCE-MRI of the breast at 3 T. We propose SRSF using Hoffmann's method of saturation as the pulse sequence (10) for this purpose.

THEORY

To minimize the effect of T_{10} variations in DCE-MRI quantification, Hittmair et al. (14) proposed an enhancement factor as the index quantified from images acquired using a FLASH pulse sequence. The Hittmair's enhancement factor ($EF_{HITTMAIR}$) is given by

$$EF_{HITTMAIR} = \frac{1}{K \cdot TR} \ln\left(\frac{S_{MAX} - S_{PRE}}{S_{MAX} - S_{POST}}\right) \quad \text{with } S_{MAX} = k \cdot M_0 \cdot \sin\alpha, \quad [2]$$

where α is flip angle, K is a correction factor dependent on α, TR is repetition time, S_{PRE} is precontrast signal, S_{POST} is postcontrast signal, k is the scanner's signal amplification factor, and M_0 is equilibrium magnetization. This index was derived by approximating the signal intensity (S) to the FLASH equation

$$S \approx S_{APPROX} = S_{MAX}\left[1 - \exp\left(-K\,\frac{TR}{T_1}\right)\right]. \quad [3]$$

Alternatively, a similar argument can be applied in the case where an SRSF sequence is used (rather than a FLASH sequence as per $EF_{HITTMAIR}$). In this case, the SRSF signal intensity can be simplified to be

$$S = k \cdot M_0\left[1 - \exp\left(-\frac{T_{REC}}{T_1}\right)\right]\sin\alpha, \quad [4]$$

where T_{REC} is the duration between the end of the saturation pulse and the first acquisition pulse in the pulse sequence. For SRSF, a proton density signal (S_{PD}) can be obtained with $T_{REC} > T_1$. Hence, the signal can be applied as an approximation of the maximum signal intensity, i.e., $S_{PD} \approx S_{MAX}$. By comparing Eq. 4 with Eq. 3, the enhancement factor using SRSF (EF_{SRSF}) can now be determined as follows:

$$EF_{SRSF} = \frac{1}{T_{REC}} \ln\left(\frac{S_{PD} - S_{PRE}}{S_{PD} - S_{POST}}\right). \quad [5]$$

The linear relationship between EF_{SRSF} and ΔR_1 can be shown as follows. By using the SRSF pulse sequence, precontrast and postcontrast signals are given by

$$S_{PRE} = S_{MAX}[1 - \exp(-T_{REC} \cdot R_{1,PRE})] \quad [6]$$

and

$$S_{POST} = S_{MAX}[1 - \exp(-T_{REC} \cdot R_{1,POST})]. \quad [7]$$

The difference between the maximum signal and precontrast and postcontrast signals are given by

$$S_{MAX} - S_{PRE} = S_{MAX} \cdot \exp(-T_{REC} \cdot R_{1,PRE}) \quad [8]$$

and

$$S_{MAX} - S_{POST} = S_{MAX} \cdot \exp(-T_{REC} \cdot R_{1,POST}). \quad [9]$$

By substituting Eqs. 8 and 9 into Eq. 5

$$EF_{SRSF} = (R_{1,POST} - R_{1,PRE}) = \Delta R_1. \quad [10]$$

Equation 10 shows that EF_{SRSF} can be directly used to quantify ΔR_1 (and thus contrast agent uptake) in a manner which is independent of T_{10}.

This enhancement factor and ΔR_1 relationship can be further simplified. By expanding with a Taylor series, for $T_{REC} < T_1$, we have

$$\exp\left(-\frac{T_{REC}}{T_1}\right) \approx 1 - \frac{T_{REC}}{T_1} = 1 - T_{REC} \cdot R_1. \quad [11]$$

Thus, by substituting Eq. 11 into Eq. 4, the signal intensity can be approximated as follows:

$$S \approx k \cdot M_0\,\frac{T_{REC}}{T_1}\sin\alpha. \quad [12]$$

For $T_{REC} < T_1$, ΔR_1 can be determined by normalizing the signal enhancement to the proton density signal. This index that is denoted as EF'_{SRSF} in this article is a simplified version of the EF_{SRSF} and given by

$$EF'_{SRSF} = \frac{1}{T_{REC}}\left(\frac{S_{POST} - S_{PRE}}{S_{PD}}\right) \approx \Delta R_1. \quad [13]$$

In theory, this simple index could be implemented on a typical image viewing workstation. The indices evaluated in this article are summarized in Table 1.

For the SRSF pulse sequence to work efficiently in the presence of B_1 transmission-field inhomogeneity, the

Table 1
Enhancement Indices with Their Respective Pulse Sequence

Index	Equation	Pulse sequence
Enhancement ratio	$\mathrm{ER} = \frac{S_{\mathrm{POST}} - S_{\mathrm{PRE}}}{S_{\mathrm{PRE}}}$	FLASH
Hittmair's enhancement factor	$\mathrm{EF}_{\mathrm{HITTMAIR}} = \frac{1}{K \cdot \mathrm{TR}} \ln\left(\frac{S_{\mathrm{MAX}} - S_{\mathrm{PRE}}}{S_{\mathrm{MAX}} - S_{\mathrm{POST}}}\right)$	FLASH
SRSF enhancement factor	$\mathrm{EF}_{\mathrm{SRSF}} = \frac{1}{T_{\mathrm{REC}}} \ln\left(\frac{S_{\mathrm{PD}} - S_{\mathrm{PRE}}}{S_{\mathrm{PD}} - S_{\mathrm{POST}}}\right)$	SRSF
Simplified SRSF enhancement factor	$\mathrm{EF}'_{\mathrm{SRSF}} = \frac{1}{T_{\mathrm{REC}}} \left(\frac{S_{\mathrm{POST}} - S_{\mathrm{PRE}}}{S_{\mathrm{PD}}}\right)$	SRSF

saturation scheme applied should be completely effective and applied immediately after the previous readout pulse train. A number of approaches have been proposed to achieve the effective saturation effect, e.g., adiabatic half-passage (15), composite (16), and saturation train (10) pulses.

METHODS

Computer Simulations

To investigate the effects of T_{10} variation on enhancement index, a DCE-MRI acquisition was simulated. This was done by assuming uptake of contrast agent over a typical range reported in breast tumors using the SRSF pulse sequence. Then, assuming a ΔR_1 proportional to concentration of contrast agent

$$\Delta R_1 = R_1 - R_{10}, \qquad [14]$$

where R_{10} and R_1 are reciprocals of the precontrast and postcontrast T_1, respectively. The enhancement indices (ER, $\mathrm{EF}_{\mathrm{HITTMAIR}}$, $\mathrm{EF}_{\mathrm{SRSF}}$, and $\mathrm{EF}'_{\mathrm{SRSF}}$) were then calculated for this range of changes in relaxation rate. For $\mathrm{EF}_{\mathrm{HITTMAIR}}$ (Eq. 3), we assumed $K = 3.05$ for an equivalent $\alpha = 35^\circ$. This was interpolated from the literature (14).

The following equation was used to simulate signal intensity acquired using FLASH sequence:

$$S = k M_0 \frac{1 - \exp(-\mathrm{TR}/T_1)}{1 - \cos\alpha \cdot \exp(-\mathrm{TR}/T_1)} \sin\alpha, \qquad [15]$$

where TR is relaxation time and α is RF flip angle. Here, echo time (TE) was assumed to be very short compared to the precontrast and postcontrast T_2^* such that T_2^* decay during acquisition is negligible. Typical parameters used in clinical breast DCE-MRI (α/TR = 35°/10 ms) were used (17) to calculate T_1-weighted signals.

For SRSF sequence that is used to calculate $\mathrm{EF}_{\mathrm{SRSF}}$ and $\mathrm{EF}'_{\mathrm{SRSF}}$, the signal intensities were determined by using

$$S = k M_0 \left[1 - \exp\left(-\frac{T_{\mathrm{REC}}}{T_1}\right)\right] \sin\alpha, \qquad [16]$$

where T_{REC} is the recovery time between the end of saturation and the first imaging pulses (we assumed signal acquisition using centric *k*-space ordering scheme). T_1 and proton density–weighted signals were determined using $T_{\mathrm{REC}} = 100$ and 2000 ms, respectively.

The effects of B_1 inhomogeneity on enhancement index were performed by simulating DCE-MRI data, as above, and using RF pulses that were 50 and 150% of their nominal pulse angles. This was done for the imaging pulses and for, the SRSF sequence, the saturation pulses. Again, ER, $\mathrm{EF}_{\mathrm{SRSF}}$, and $\mathrm{EF}'_{\mathrm{SRSF}}$ were calculated.

For the quantification of $\mathrm{EF}_{\mathrm{SRSF}}$ and $\mathrm{EF}'_{\mathrm{SRSF}}$ using the SRSF pulse sequence, a longer scanning time is expected. To minimize the scanning time by using this pulse sequence, a short T_{REC} both in the T_1-weighted and proton density–weighted image acquisitions is desirable. Hence, the relationship between the indices and ΔR_1 was evaluated by using different T_{REC}s. All computer simulations were performed using Matlab (Mathworks, Inc., Natick, USA).

Imaging Experiments

To validate the computer simulations, a series of imaging experiments were performed on a set of T_1 gel phantoms, which were prepared using methods used by Walker et al. (18) and Waiter and Foster (19). These phantoms represent typical T_1 values of the precontrast and postcontrast breast tissues at 3 T (20). T_1 values were determined using inversion-recovery fast spin-echo (IR-FSE) pulse sequence. Values of T_1 and S_0 were estimated by fitting the following function to the observed signal intensity:

$$S = S_0 \left[1 - 2\exp\left(-\frac{T_{\mathrm{REC}}}{T_1}\right)\right], \qquad [17]$$

where S_0 is the signal for $T_{\mathrm{REC}} > T_1$.

To achieve the effective saturation effect in the presence of B_1 inhomogeneity in the SRSF pulse sequence, Hoffmann's method of saturation pulses (10) was used. The technique uses a series of six nonselective 90° hard RF pulses separated by a decreasing duration of delays and spoiling gradients. The saturation scheme was applied immediately after the readout pulses.

Using ImageJ (National Institute of Health, Bethesda, USA), signal intensity values were measured from regions-of-interest in each gel phantoms in the central (10th) slice of a 3D data set. Measurement of the effect of T_{10} variation on the enhancement indices was done by assuming that different T_{10}s (and hence S_{PRE}) correspond to the gel phantoms with the longer T_1 values and then assuming that the remaining phantoms with $T_1 < T_{10}$ represent tissues with shorter postcontrast T_1 values. The proton density signal (S_{PD}) was determined by averaging the signal intensities of all the gel phantoms in the proton density signal–weighted images. From these signal values, ER (using T_1-weighted FLASH), $\mathrm{EF}_{\mathrm{SRSF}}$, and $\mathrm{EF}'_{\mathrm{SRSF}}$ (using T_1-weighted and proton density–weighted SRSF) were calculated. Changes in relaxation rate (ΔR_1) for the gel phantoms were calculated using Eq. 14. The effect of B_1 inhomogeneity on the measurement of ER,

Table 2
Imaging Parameters Used in the Imaging Experiments on Gel Phantoms

Parameter	IR-FSE	SRSF	FLASH
Technique	2D	3D	3D
T_{REC} (ms)	50, 150, 350, 700, and 1400	100 ms (T_1-weighted) and 2000 (PD-weighted)	Nil
α (°)	90	12	35
TR (ms)	7000	4.1	10
TE (ms)	18	2.3	2.3
Voxel size (mm)	1 × 1 × 10	1 × 1 × 1	1 × 1 × 1
FOV (mm)	200 × 200	200 × 200	200 × 200
No. of slices	1	20	20
Echo-train-length	6	50	1

Table 3
Imaging Parameters Used in the Imaging on a Volunteer and the Respective Imaging Time

Parameter	T_1-w SRSF	PD-w SRSF	T_1-w FLASH
T_{REC} (ms)	100	2000	Nil
α (°)	12	12	35
TR (ms)	4.4	4.4	11
TE (ms)	2.3	2.3	2.3
Voxel size (mm)	1 × 1 × 1	1 × 1 × 1	1 × 1 × 1
FOV (mm)	340 × 340	340 × 340	340 × 340
No. of slices	150	150	150
Echo-train-length	50	50	50
SENSE	Yes[a]	Yes[a]	Yes[a]
Imaging time	51 s	5 min 18 s	1 min 8 s

[a]A SENSE factor of 2 was applied in both the right-left and foot-head directions.

EF_{SRSF}, and EF'_{SRSF} was then evaluated. This was done by imaging the same phantoms using RF pulses that were 50 and 150% of their nominal pulse angles as for the simulations (i.e., 35° for FLASH, and 90° preparation and 12° read-out pulses for SRSF sequences).

For comparison, SRSF with a 90° hard RF pulse followed by spoiling gradients before the read-out scheme was also performed. For this study, the B_1 inhomogeneity was applied only in the read-out scheme. Hence, an SRSF sequence with completely effective saturation was assumed being acquired. Again, ER, EF_{SRSF}, and EF'_{SRSF} were calculated. All imaging experiments were performed using a Philips Achieva X-series 3.0-T scanner and a transmit-receive birdcage quadrature head coil (Philips

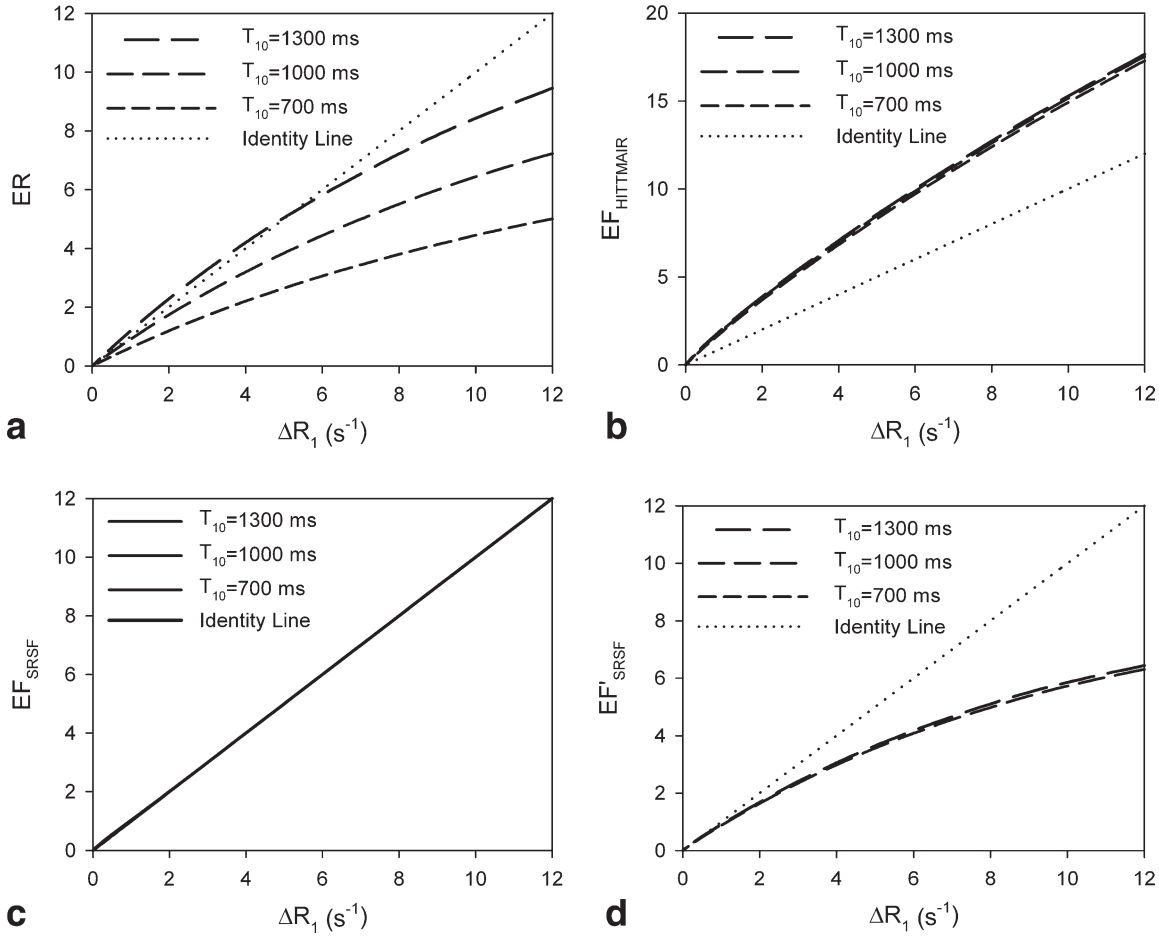

FIG. 1. The effect of different native T_1s (T_{10}) on enhancement indices, where (**a**) ER (α = 35° and TR = 10 ms), (**b**) $EF_{HITTMAIR}$ (α = 35°, TR = 10 ms, and K = 3.05), (**c**) EF_{SRSF}, and (**d**) EF'_{SRSF}. For (c) and (d), α = 12°, T_{REC} (T_1-weighted) = 100 ms, and T_{REC} (PD-weighted) = 2000 ms were used.

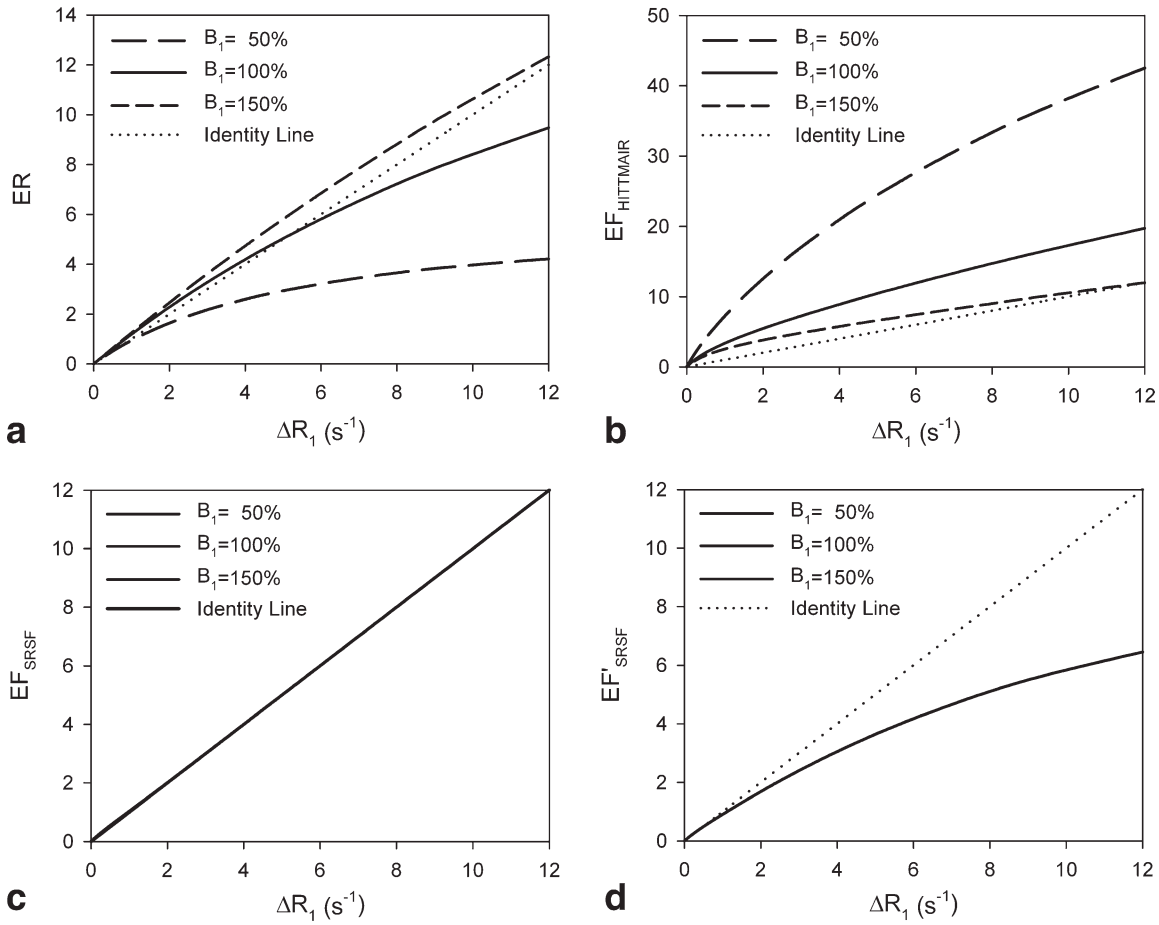

FIG. 2. The effect of B_1 transmission-field inhomogeneity on (**a**) ER ($\alpha = 35^\circ$ and TR = 10 ms), (**b**) $EF_{HITTMAIR}$ ($\alpha = 35^\circ$, TR = 10 ms, and $K = 3.05$), (**c**) EF_{SRSF}, and (**d**) EF'_{SRSF}. For (c) and (d), $\alpha = 12^\circ$, T_{REC} (T_1-weighted) = 100 ms, and T_{REC} (proton density–weighted) = 2000 ms were used. Note that the plots in (c) and (d) overlap so that they are virtually indistinguishable.

Healthcare, Best, The Netherlands). The head coil was used instead of breast coil because of its ability to produce a homogeneous B_1 transmission field across a transaxial section through its center (8). Hence, all phantoms were assumed to be subject to the same amplitude of B_1 transmission field. The parameters used in the imaging experiments are given in Table 2. To determine the noise (uncertainty) for the images produced using different imaging techniques, the standard deviation from four regions-of-interest was measured outside the gel phantoms in the image (i.e., in air). The SNR was calculated by dividing the mean signal intensity of the shortest T_1 gel phantom with the average noise value across the four regions-of-interest. The ratios between the enhancement indices and the uncertainty were then calculated.

To simulate the clinical situation, the T_1-weighted SRSF, proton density–weighted SRSF, and T_1-weighted FLASH 3D imaging were also performed on a healthy female volunteer after ethical approval by a local ethics committees, and informed consent was obtained. The subject was positioned prone and head first inside the scanner and imaged axially with a seven-channel sensitivity-encoding (SENSE) breast coil (Philips Healthcare, Best, The Netherlands). Imaging parameters used are given in Table 3.

RESULTS

Computer Simulations

The effect of T_{10} variation on ER, $EF_{HITTMAIR}$, EF_{SRSF}, and EF'_{SRSF} is shown in Fig. 1. Here, ΔR_1 was assumed to be directly proportional to the contrast agent uptake within the tissue. In theory, an enhancement index that is insensitive to the T_{10} variation will have the same curve of enhancement versus ΔR_1 regardless of the value of T_{10}. The closer the curves lay to each other on Fig. 1, the less the index is influenced by the T_{10} variation. Hence, from the figure, $EF_{HITTMAIR}$, EF_{SRSF}, and EF'_{SRSF} are much less sensitive to T_{10} variation compared to ER. The range of ΔR_1 was chosen to cover a wide range of ΔR_1 expected in breast cancers.

The effect of B_1 inhomogeneity on the enhancement indices is shown in Fig. 2. The closer the curves lay to each other on Fig. 2, the less the index is affected by the B_1 inhomogeneity. Hence, ER and $EF_{HITTMAIR}$ (both using a FLASH sequence) are significantly influenced by the B_1 error. However, EF_{SRSF} and EF'_{SRSF} are not affected by B_1 inhomogeneity.

Figure 3 shows the relationship between the SRSF enhancement factors and ΔR_1 by using different proton density–weighted T_{REC}. The closer the curve to the identity line shows more similarity between the index and

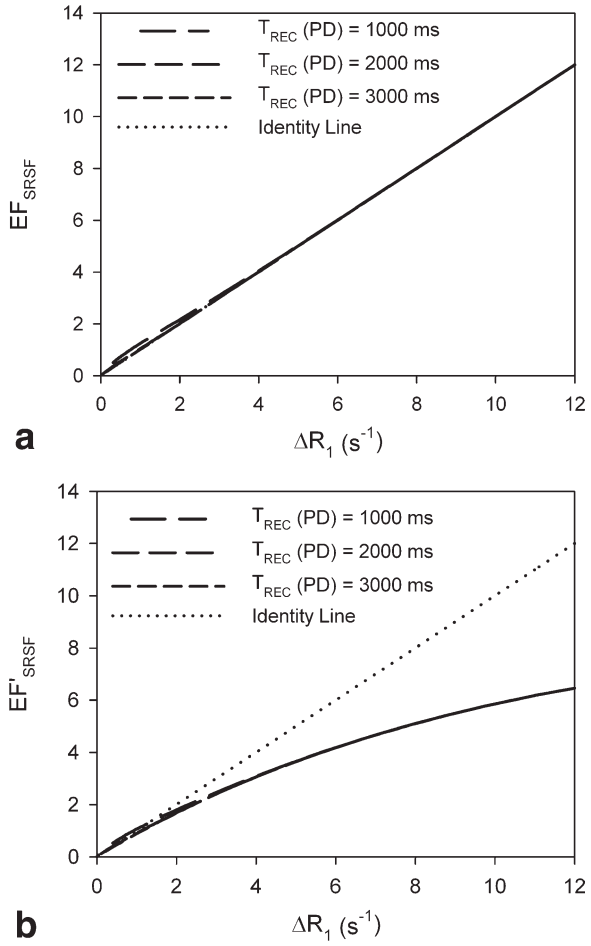

FIG. 3. SRSF enhancement indices simulated by using different proton density (PD)-weighted T_{REC}, where (**a**) EF_{SRSF} and (**b**) EF'_{SRSF} (T_1-weighted T_{REC} = 100 ms and native T_1 = 1300 ms were assumed).

ΔR_1. In general, a better index and ΔR_1 value similarity can be obtained by using a longer T_{REC} in proton density image acquisition. However, for the range of the proton density T_{REC} used in the simulation, the effect of shorter T_{REC} to the index-ΔR_1 identity is minimal especially in the calculation of EF'_{SRSF}. The index-ΔR_1 mismatch is more prevalent at a smaller ΔR_1 range.

The effect of using different T_1-weighted T_{REC} is shown in Fig. 4. A very small difference was observed when different T_1-weighted T_{REC}s were used to calculate EF_{SRSF}. However, for EF'_{SRSF}, a significant decrease in index-ΔR_1 identity was observed for a longer T_{REC}.

Imaging Experiments

By using 2D IR-FSE pulse sequence, the T_1 values for the gel phantoms were found to be 89, 180, 366, 559, 800, 962, and 1266 ms. These values have a good correlation with breast tissue T_1 at 3 T (19).

Figure 5a,b shows the effect of a variation of T_{10} on EF_{SRSF} and EF'_{SRSF}. Both indices were calculated from images acquired by using Hoffmann's SRSF. ER calculated by using FLASH images is shown in Fig. 5c as comparison. The figures show that the effect of a variation in T_{10} on EF_{SRSF} and EF'_{SRSF} is minimal, whereas ER is significantly affected by the T_{10} variation. For example at ΔR_1 of 8 s^{-1}, the difference between ER calculated using T_{10} values of 1266 and 566 ms is 58%. However, <1 and 12% differences were observed for EF_{SRSF} and EF'_{SRSF}, respectively.

Figure 6a,b, respectively, shows the effect of B_1 inhomogeneity on the EF_{SRSF} and EF'_{SRSF} calculated using Hoffmann's SRSF images. The indices calculated using SRSF with an effective 90° saturation pulse are shown in Fig. 6c,d, whereas ER using FLASH sequence images is shown in Fig. 6e as comparison. From the figures, the effect of B_1 inhomogeneity on EF_{SRSF} and EF'_{SRSF} calculated from images obtained by using Hoffmann's SRSF is much less in comparison to the common ER (with FLASH sequence). At a ΔR_1 of 8 s^{-1}, a 50% reduction in the B_1 field reduces the ER by 51%, whereas for EF_{SRSF} and EF'_{SRSF} the index increases by 20 and 8%, respectively. Theoretically, the enhancement indices are unaffected by the B_1 error if a perfect saturation can be achieved in the saturation scheme of the SRSF sequence (Fig. 6c,d). Note that the values of ER, EF_{SRSF} and

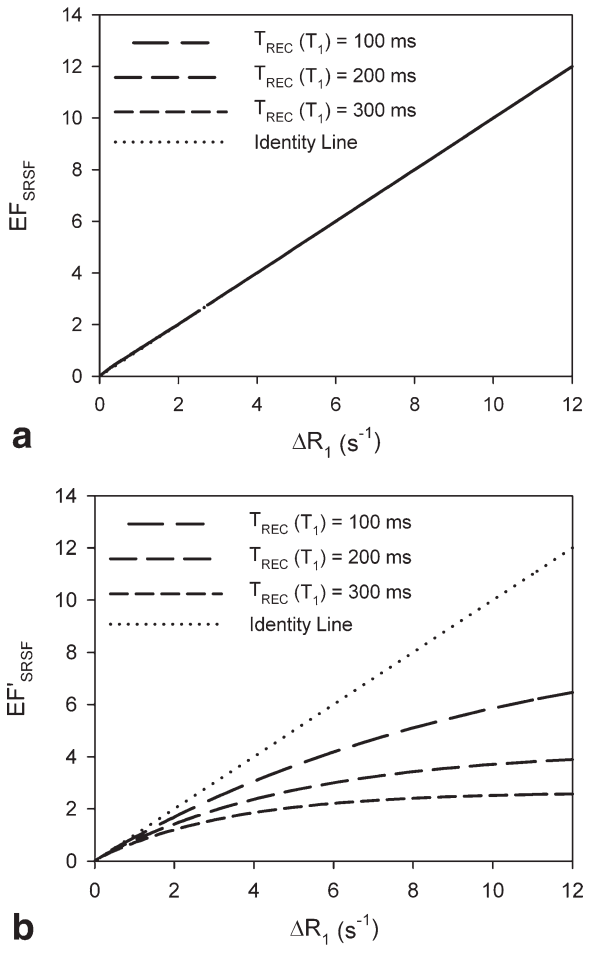

FIG. 4. SRSF enhancement indices simulated by using different T_1-weighted T_{REC}, where (**a**) EF_{SRSF} and (**b**) EF'_{SRSF} (proton density–weighted T_{REC} = 100 ms and native T_1 = 1300 ms were assumed).

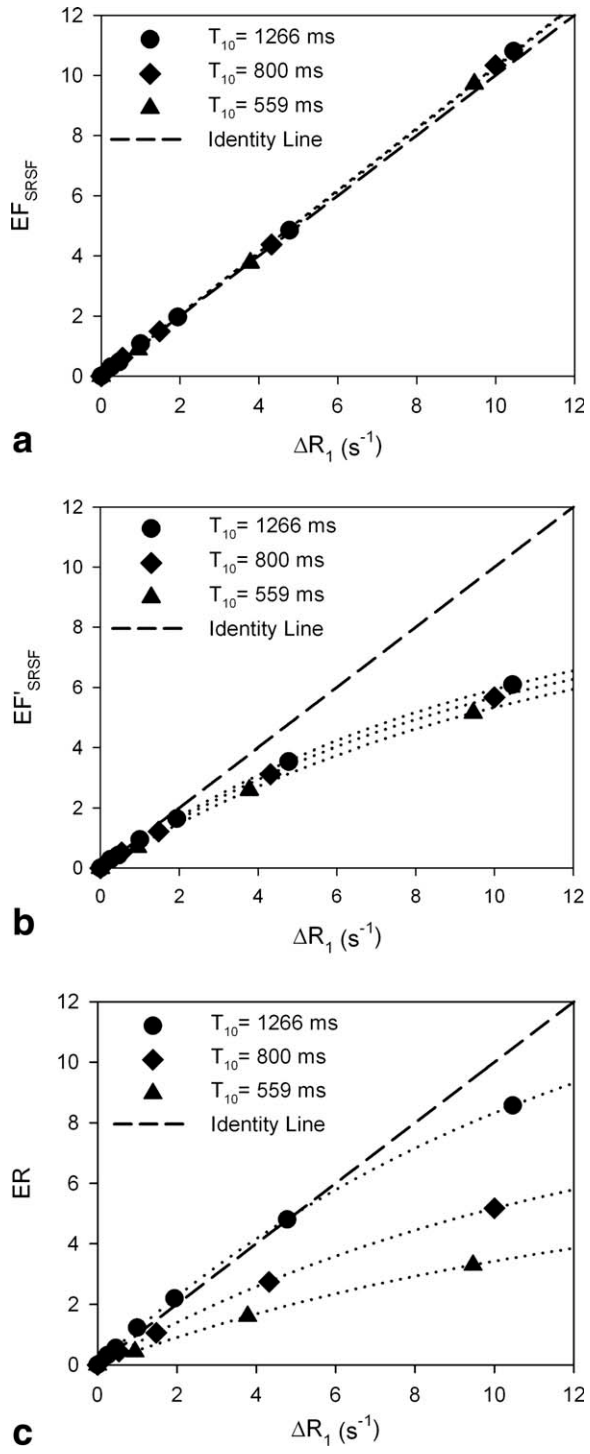

FIG. 5. The effect of different native T_1 (T_{10}) on enhancement indices using two different pulse sequences, where (**a**) EF_{SRSF} using Hoffmann's SRSF, (**b**) EF'_{SRSF} using Hoffmann's SRSF, and (**c**) ER using FLASH. The dotted lines are the fitted lines of the plotted enhancement indices.

EF'_{SRSF} at $\Delta R_1 = 8\ s^{-1}$, $T_{10} = 1266$ ms and $B_1 = 100\%$ are 7.1, 8.2 and 5.2 respectively.

The means and uncertainties of the signal intensities and EF_{SRSF}, EF'_{SRSF}, and ER are given in Table 4. By using the parameters used in the phantom experiments, the SNR (given by the mean/uncertainty ratio) for T_1-weighted imaging using Hoffmann's SRSF sequence is slightly lower compared to imaging using FLASH sequence. However, the mean/uncertainty ratios of EF_{SRSF} and EF'_{SRSF} are substantially higher compared to ER. This is due to the higher SNR of the S_{PD} signals acquired using the SRSF pulse sequence.

Figure 7 shows typical images of the breast for T_1-weighted SRSF, proton density–weighted SRSF, and FLASH pulse sequences acquired on a healthy volunteer.

DISCUSSION

In DCE-MRI of the breast, ER calculated using a FLASH pulse sequence is a commonly used enhancement index to evaluate breast cancers. We have shown that this index is significantly affected by the variation of tissue's T_{10}. Tissues with a short T_{10} have a low ER values and vice versa (Fig. 1a). This issue can be minimized by using $EF_{HITTMAIR}$, which is an alternative index introduced by Hittmair et al. (Fig. 1b) (14). Like ER, $EF_{HITTMAIR}$ is also calculated on images acquired using a FLASH pulse sequence. However, the main limitation of this index is that it is significantly affected by B_1 inhomogeneity (Fig. 2b), which is a significant problem at 3 T. It has been shown that the B_1 field can be reduced to about one-half of the nominal field in one side of the breast at 3 T (7,8). However, contrary to the ER, a lower B_1 increases the $EF_{HITTMAIR}$ and vice versa.

To minimize the effect of both the variation of tissue's T_{10} and the B_1 inhomogeneity in DCE-MRI at 3 T, we propose a new approach to quantify the contrast agent uptake. This technique involves new enhancement indices namely EF_{SRSF} and EF'_{SRSF}, which were calculated on images acquired using an SRSF pulse sequence. EF_{SRSF} is a modification of $EF_{HITTMAIR}$ specifically developed to be used with SRSF pulse sequence. Like Hittmair's index, the EF_{SRSF} requires the calculation of natural log, which may be difficult to perform using a standard clinical workstation. Therefore, this index is more likely to be used by the manufacturer as part of their analysis product or by research personnel in the viewing or independent workstation. As an alternative, we also introduced another index called EF'_{SRSF}, which is simpler to implement on a typical viewing workstation. Both of these indices have much less sensitivity to the variation of T_{10} and B_1 inhomogeneity compared to the ER. This is demonstrated in this work by computer simulation (Figs. 1 and 2) and imaging experiments (Figs. 5 and 6). Like $EF_{HITTMAIR}$, both indices require the acquisition of T_1-weighted and proton density–weighted images.

We used Hoffmann's method of preparation scheme (10) to produce saturation in the presence of B_1 inhomogeneity. By using this technique much less error in the EF_{SRSF} and EF'_{SRSF} was observed (Fig. 6a,b) compared to the ER acquired using the FLASH sequence (Fig. 6e) in the presence of B_1 inhomogeneity. The error in EF_{SRSF} and EF'_{SRSF} is mainly contributed by the imperfection in Hoffmann's saturation technique in producing a perfect saturation in the presence of B_1 inhomogeneity. Less error in both indices can be obtained if a better saturation scheme is used in the SRSF pulse sequence (Fig. 6c,d).

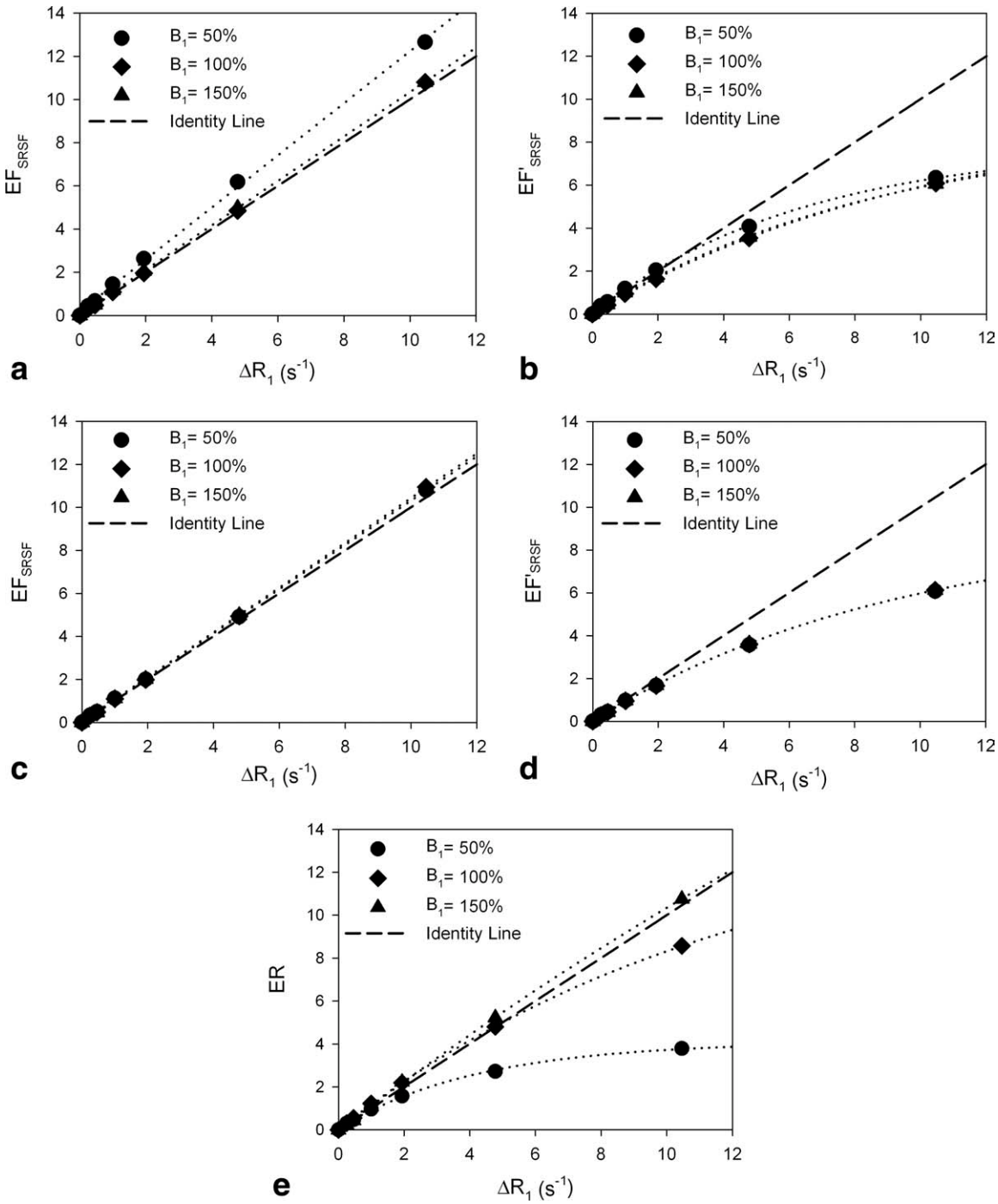

FIG. 6. The effect of B_1 transmission-field inhomogeneity on the enhancement indices using two different pulse sequences, where (**a**) EF_{SRSF} using Hoffmann's SRSF, (**b**) EF'_{SRSF} using Hoffmann's SRSF, (**c**) EF_{SRSF} using SRSF with an effective 90° saturation pulse, (**d**) EF'_{SRSF} using SRSF with an effective 90° saturation pulse, and (**e**) ER using FLASH. The dotted lines are the fitted lines of the plotted enhancement indices.

Another advantage of EF_{SRSF} and EF'_{SRSF} compared to $EF_{HITTMAIR}$ is that the indices do not require the correction factor K in the calculation (Eq. 2). Because the factor is dependent on the flip angle (and hence the B_1), less error in the indices can be obtained in the presence of B_1 inhomogeneity by omitting the K factor. Furthermore, although it was not investigated in this article, a similar argument indicates that EF_{SRSF} and EF'_{SRSF} will not be affected by slice profile effects in 2D implementations of the methods, as compared to $EF_{HITTMAIR}$ which may be. As shown by the simulations of Figs. 1c and 2c, EF_{SRSF} equals ΔR_1. This is confirmed to a good approximation by the experimental data of Figs. 5a and 6a. Hence, the index can be used as a direct quantification of the contrast agent uptake. This is a major benefit of EF_{SRSF}. However, unlike EF_{SRSF}, EF'_{SRSF} is not linear with the

Table 4
Mean and Uncertainty Values of Signal Intensities and Enhancement Indices Measured or Calculated from Gel Phantoms Images

Pulse sequence	Signal or enhancement index	Mean	Uncertainty	Mean/Uncertainty
Hoffmann's SRSF	S_{PRE}	1.25×10^5	1.32×10^4	9.53
	S_{POST}	1.09×10^6	1.32×10^4	83.28
	S_{PD}	1.60×10^6	1.35×10^4	118.14
	EF_{SRSF}	10.80	0.10	103.85
	EF'_{SRSF}	6.07	0.04	151.75
FLASH	S_{PRE}	1.84×10^4	1.48×10^3	12.37
	S_{POST}	1.77×10^5	1.48×10^3	119.25
	ER	8.60	0.70	12.30

ΔR_1 (Figs. 1d and 2d). Hence, EF'_{SRSF} should be used like ER and $EF_{HITTMAIR}$ (with $\alpha = 35°$) where standard acquisition parameters must be used during imaging so that the index can be compared between different patients, scanners, and imaging centers.

Images acquired on a volunteer show that the T_1-weighted image quality is comparable to that obtained with typical FLASH parameters (see Fig. 7). Even though the SNR produced in the T_1-weighted images was slightly lower compared to the FLASH, the ratio between the enhancement index and the uncertainty calculated from the noise levels is substantially higher than the ER (see Table 4). This is due to the higher SNR of the proton density images acquired using SRSF pulse sequence. From our experience of imaging on several volunteers, the image quality in the proton density images is not substantially affected by the patient motion (assuming that the subject lies in prone position).

The main drawback of the new DCE-MRI quantification approach is the longer total scanning time is required compared to the common technique, i.e., ER with FLASH. This time penalty is contributed by an additional scanning protocol to acquire the proton density–weighted images for the calculation of the indices. Furthermore, the SRSF pulse sequence requires a delay between the saturation pulse and the image acquisition. A much longer recovery time is needed for the acquisition of proton density–weighted images ($T_{REC} > T_1$) compared to T_1-weighted images ($T_{REC} < T_1$).

The SRSF imaging time can be reduced by optimizing the acquisition parameters of the pulse sequence, e.g., by using a very short TR. This is performed by using a very low flip angle in the image acquisition. Because the contrast in the SRSF pulse sequence is mainly contributed by the T_1 and T_{REC} (Eq. 4), multiple signal acquisitions (echo train) can be performed after a saturation pulse. This is useful to reduce the imaging time. For example, we performed 50 signal acquisitions (echo-train-length) after the saturation scheme in the SRSF experiment. A longer echo-train-length will reduce the time further at the cost of increasing the index error.

Another time reduction approach is to use the shortest T_{REC} as possible both in the T_1- and proton density–weighted image acquisitions. By using the imaging parameters used in this work (see Table 3), the scanning time for the T_1-weighted imaging using the SRSF pulse sequence is shorter (by a quarter) than the typical FLASH. However, a much longer time is required for the proton density–weighted imaging (>5 min). This is due to the long T_{REC} is necessary to produce the proton density–weighted signals. Decreasing T_{REC} in proton density image acquisition will reduce the index-ΔR_1 identity relationship (see Fig. 3). This effect is caused by the fact that there is more T_1 weighting component introduced in the image and so will also influence the indices calculated. A shorter T_{REC} in the T_1-weighted image acquisition will improve the index-ΔR_1 identity relationship (Fig. 4), but it will reduce the SNR. Therefore, an optimum T_{REC} for both the T_1- and proton density–weighted

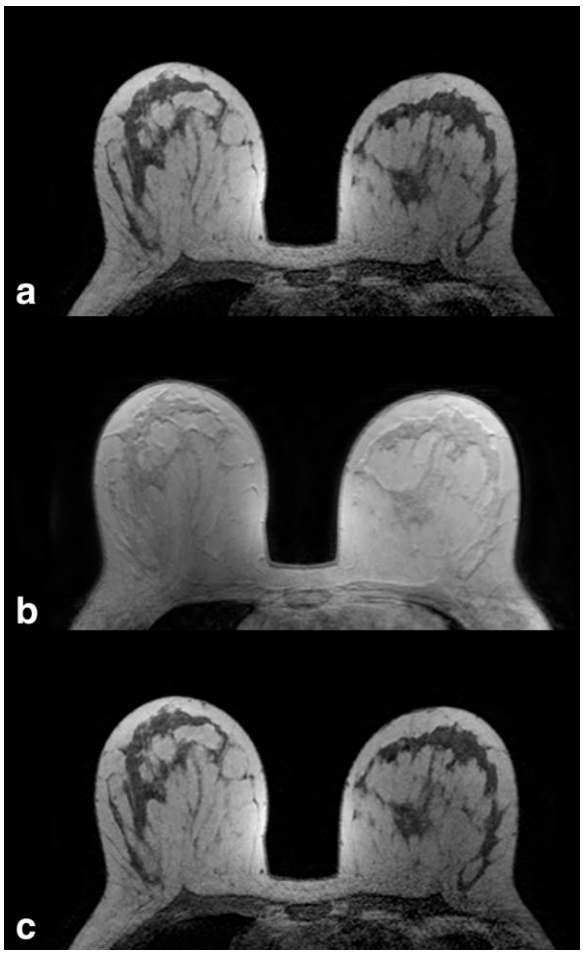

FIG. 7. Typical images of the breast acquired on a volunteer using: (**a**) T_1-weighted Hoffmann's SRSF, (**b**) proton density–weighted Hoffmann's SRSF, and (**c**) T_1-weighted FLASH pulse sequences.

image acquisitions should be used. For example, in this work, we used T_{REC} of 100 and 2000 ms for the T_1-weighted and proton density–weighted imaging, respectively.

The extra time penalty due to performing the proton density–weighted imaging is compensated by avoiding imaging to measure the tissues' T_{10} as commonly performed in pharmacokinetics studies. Note that it is possible to improve the index/uncertainty ratio for ER to the same level of EF_{SRSF} and EF'_{SRSF} with this extra time. This can be done by improving the SNR in the precontrast T_1-weighted FLASH, e.g., by using several numbers of signals averaging in the imaging. Other fast MRI approaches such as SENSE (21) (as implemented in the in vivo imaging), dynamic keyhole (22), and compressed sensing (23) may also be beneficial to reduce the scanning time even further.

CONCLUSION

New enhancement indices, i.e., EF_{SRSF} and EF'_{SRSF}, to quantify contrast agent uptake in DCE-MRI of the breast have been tested. These indices were calculated from T_1 and proton density–weighted images acquired using a SRSF pulse sequence. Compared to conventional enhancement indices that compare signal change against pre-enhancement signal values, these new indices are considerably less affected by errors caused by variations in the T_{10} of different tissues and by B_1 transmission-field inhomogeneity. The methods are also expected to have applications in other organs and at field strengths at 3 T and above.

ACKNOWLEDGMENT

The authors thank Dr. Matthew Clemence of Philips Healthcare for his support on this work.

REFERENCES

1. Boetes C, Barentsz JO, Mus RD, Van der Sluis RF, Van Erning LJTO, Hendriks JHCL, Holland R, Ruys SHJ. MR characterization of suspicious breast lesions with a gadolinium-enhanced TurboFLASH subtraction technique. Radiology 1994;193:777–781.
2. Heywang-Köbrunner SH, Viehweg P, Heinig A, Küchler C. Contrast-enhanced MRI of the breast: accuracy, value, controversies, solutions. Eur Radiol 1997;24:94–108.
3. Kuhl CK, Schrading S, Leutner CC, Morakkabati-Spitz N, Wardelmann E, Fimmers R, Kuhn W, Schild HH. Mammography, breast ultrasound, and magnetic resonance imaging for surveillance of women at high familial risk for breast cancer. J Clin Oncol 2005;23: 8469–8476.
4. Tofts PS. Modeling tracer kinetics in dynamic gd-DTPA MR imaging. J Magn Reson Imaging 1997;7:91–101.
5. Brookes JA, Redpath TW, Gilbert FJ, Murray AD, Staff RT. Accuracy of T1 measurement in dynamic contrast-enhanced breast MRI using two- and three-dimensional variable flip angle fast low-angle shot. J Magn Reson Imaging 1999;9:163–171.
6. Preibisch C, Deichmann R. Influence of RF spoiling on the stability and accuracy of T1 mapping based on spoiled FLASH with varying flip angles. Magn Reson Med 2009;61:125–135.
7. Kuhl CK, Kooijman H, Gieseke J, Schild HH. Effect of B_1 inhomogeneity on breast MR imaging at 3.0 T. Radiology 2007;244:929–930.
8. Azlan CA, Di Giovanni P, Ahearn TS, Semple SIK, Gilbert FJ, Redpath TW. B_1 transmission-field inhomogeneity and enhancement ratio errors in dynamic contrast-enhanced MRI (DCE-MRI) of the breast at 3T. J Magn Reson Imaging 2010;31:234–239.
9. Di Giovanni P, Azlan CA, Ahearn TS, Semple SI, Gilbert FJ, Redpath TW. The accuracy of pharmacokinetic parameter measurement in DCE-MRI of the breast at 3 T. Phys Med Biol 2010;55:121–132.
10. Hoffmann U, Brix G, Knopp MV, Hess T, Lorenz WJ. Pharmacokinetic mapping of the breast: a new method for dynamic MR mammography. Magn Reson Med 1995;33:506–514.
11. Parker GJ, Baustert I, Tanner SF, Leach MO. Improving image quality and T(1) measurements using saturation recovery turboFLASH with an approximate K-space normalization filter. Magn Reson Med 2000; 18:157–167.
12. Kim D, Gonen O, Oesingmann N, Axel L. Comparison of the effectiveness of saturation pulses in the heart at 3T. Magn Reson Med 2008;59:209–215.
13. Azlan CA, Ahearn TS, Di Giovanni P, Semple SI, Gilbert FJ, Redpath TW. Saturation-recovery snapshot FLASH reduces RF pulse angle inhomogeneity artefacts in DCE-MRI of the breast at 3T. In: Proceedings of the Joint Annual Meeting of ISMRM-ESMRMB, Stockholm, 2010. p 2492.
14. Hittmair K, Gomiscek G, Langenberger K, Recht M, Imhof H, Kramer J. Method for the quantitative assessment of contrast agent uptake in dynamic contrast-enhanced MRI. Magn Reson Med 1994;31:567–571.
15. Tannús A, Garwood M. Adiabatic pulses. NMR Biomed 1997;10: 423–434.
16. Grant DM, Harris RK. Encyclopedia of nuclear magnetic resonance. Sussex, England: Wiley; 1996. pp 1396–1410.
17. Warren RML, Pointon L, Thompson D, Hoff R, Gilbert FJ, Padhani A, Easton D, Lakhani SR, Leach MO. Reading protocol for dynamic contrast-enhanced MR images of the breast: sensitivity and specificity analysis. Radiology 2005;236:779–788.
18. Walker P, Lerski RA, Mathur-De Vre R, Yane F. Preparation of agarose gels as reference substances for NMR relaxation time measurement. Magn Reson Imaging 1988;6:215–222.
19. Waiter GD, Foster MA. Lanthanide-EDTA doped agarose gels for use in NMR imaging phantoms. Magn Reson Imaging 1997;15:929–938.
20. Rakow-Penner R, Daniel B, Yu H, Sawyer-Glover A, Glover GH. Relaxation times of breast tissue at 1.5T and 3T measured using IDEAL. J Magn Reson Imaging 2006;23:87–91.
21. Pruessmann KP, Weiger M, Scheidegger MB, Boesiger P. SENSE: sensitivity encoding for fast MRI. Magn Reson Med 1999;42:952–962.
22. Spraggins TA. Simulation of spatial and contrast distortions in keyhole imaging. Magn Reson Med 1994;31:320–322.
23. Lustig M, Donoho D, Pauly JM. Sparse MRI: the application of compressed sensing for rapid MR imaging. Magn Reson Med 2007;58: 1182–1195.